



Impedance Plethysmography for Respiratory Flow and Rate Estimation using Multilayer Perceptrons

Michael Klum^a, Timo Tigges^a, Alexandru-Gabriel Pielmus^a, Aarne Feldheiser^b,
and Reinhold Orglmeister^a

^aTechnische Universität Berlin, Chair of Electronics and Medical Signal Processing, Berlin, Germany

^bUniversitätsklinikum Essen und Universität Duisburg-Essen, Klinik für Anästhesiologie und Intensivmedizin, Essen, Germany

Correspondence: Michael Klum, Technische Universität Berlin, Chair of Electronics and Medical Signal Processing, Einsteinufer 17, 10587 Berlin, Germany

E-mail: michael.klum@tu-berlin.de Website: <https://www.emsp.tu-berlin.de> Phone: +49 (0) 30 314 23889

Abstract. Highly integrated analog frontends for biosignal acquisition facilitate the development of complex yet small vital sign monitors capable of passive sensing. However, the established gold standards for sensor positioning cover large areas of the patient's body. Especially when measuring respiration, an important parameter in postoperative care and sleep monitoring, masks, belts or nasal cannulas are used. Therefore, estimation techniques such as photoplethysmography (PPG) derived respiration have emerged. Fingertip PPG is a widely used modality acquired optically at the peripheral vascular system. While miniaturized reflective PPG systems are available, their integration can prove problematic in certain scenarios, especially with textiles. We propose impedance plethysmography as a well integrable alternative to PPG for the estimation of absolute respiratory flow and rate. Employing nested cross-validation and wrapper techniques in a model and feature selection framework, we analyzed different polynomial and multilayer perceptron regression models as well as feature sets. In a pilot study, we achieved relative errors of 1.5 % for respiratory rate and 59 % for flow estimation using seven time-domain features of the acquired impedance signal. We conclude that impedance plethysmography can be a promising alternative for highly integrated and unobtrusive respiratory rate estimation as well as rough flow estimation.

Keywords: Impedance Plethysmography; Respiratory Rate; Respiratory Flow; Model Selection; Feature Selection; Wearable; Neural Networks; Multiple Linear Regression; Unobtrusive Monitoring;

1. Introduction

Unobtrusive monitoring of biosignals without additional patient effort can potentially overcome numerous disadvantages of established approaches such as cost, discomfort, and availability as shown in the context of sleep monitoring (Tal, Shinar, Shaki, Codish, & Goldbart, 2017). For patients suffering from mental illnesses, passive sensing is a valuable option for disease management (Cornet & Holden, 2018). Textile and patch integration lead to a variety of applications, such as optimization of athletic training (Cardinale & Varley, 2017), monitoring for firefighters (Hertleer, Odhiambo, & Van Langenhove, 2013) or attention monitoring for drivers (Ramasamy, Oh, Harbaugh, & Varadan, 2013). With increasing miniaturization, it is possible to develop multimodal data acquisition systems in very small form factors. However, the sensor positioning usually requires body spanning placement of electrodes, clips, and belts. An example is the Einthoven electrocardiogram (ECG) lead system, which spans the full thorax, even though full ECG frontends are available in a single integrated circuit.

In the postanesthesia care unit, respiratory complications are the main cause of major morbidity and increased mortality (Rose, Cohen, Wigglesworth, & DeBoer, 1994). Prolonged phases of respiratory instability can persist throughout the general care ward (Broens, et al., 2017) where comparatively low recording intervals lead to missing 90% of hypoxemic episodes (Sun, et al., 2015). Respiration measurements are usually performed using nasal cannula pressure sensors, belts or masks

which reduce both compliance and comfort. Using ECG derived respiration, a less obtrusive option is available, even for electrode distances as low as 24 mm (Klum, Minn, Tigges, Pielmus, & Orglmeister, 2016). Impedance pneumography (IP) is another monitoring option which can be employed with electrode distances down to 8 cm for respiratory flow estimation (Klum, Schenck, Pielmus, Tigges, & Orglmeister, 2018). However, both ECG and IP techniques require electrodes on the patient's chest. A less obtrusive monitoring option is the use of fingertip photoplethysmography (PPG) signals to estimate respiratory parameters. When combined with ECG signals, the quality of the estimates can be improved significantly (Charlton, et al., 2016). Even though reflective PPG systems are available in very small form factors, their integration in textile systems (Zeng, et al., 2014) can still prove difficult.

It was shown that impedance changes of limb segments are caused predominantly by changes in blood volume (Schwan, 1955). As a result, impedance plethysmography (IPG) can be employed to estimate blood volume changes in peripheral vascular systems (Brown, Pryce, Baumber, & Clarke, 1975) such as the arms (Nyboer, Kreider, & Hannapel, 1950), which enables us to use it as a potentially less obtrusive and easy to integrate replacement for PPG. It has further been shown that pulse-to-pulse variations are mainly caused by the respiratory cycle (Jaffrin & Vanhoutte, 1979; Marks, 1987). Impedance plethysmography also has applications in disease assessment such as venous outflow obstruction (Anderson, 1984), deep vein thromboses and other vascular diseases (Varaki, Gargiulo, Penkala, & Breen, 2018). With increasing interest in wearables, additional research has been conducted in the field of IPG. Cho et al. presented the application of six 1.5 cm x 0.5 cm electrodes, in contrast to electrodes which encircle the whole limb (Cho, Kim, & Cho, 2009). By employing a 3D model simulation, Jivet reported transversal electrode configurations to be advantageous over linear patterns with respect to arterial segments (Jivet, 2014). Schneider et al. improved upon the analog frontend to handle unknown impedances (Schneider, Schroth, Holzhey, Blöcher, & Stork, 2017). They embedded their frontend into a wrist-worn wearable for sleep monitoring (Schneider, Schroth, Ottenbacher, & Stork, 2018). Huynh et al. employed two sets of transversal tetrapolar electrode configurations with distances down to 1 cm to assess the pulse wave velocity (Huynh, Jafari, & Chung, 2018).

We recently showed that plethysmographic signals acquired using impedance measurements at the forearm can be used to estimate the respiratory rate (Klum, Osterland, Pielmus, Tigges, & Orglmeister, 2018). In this work, we aim to extend our research to the estimation of respiratory flow using polynomial regression models and multilayer perceptrons. Our work is structured as follows: in Section 2 we first give a brief overview of the aim and the methodology of our research, followed by a description of the acquisition system, pilot study and signal pre-processing. We then describe the used features, the regression models and the performance metrics. We close the section with a detailed description of a model and feature selection framework. In Section 3 we present the results of the model and feature selection as well as the respiratory flow and rate estimation. Section 4 discusses the obtained results and lists limitations. Finally, Section 5 closes with a summary and conclusion

2. Materials and Methods

2.1 Aim and Conceptual Overview

Our aim was to estimate the respiratory flow and rate from time-domain features of vascular impedance plethysmography signals acquired at the forearm. A methodological overview over the signal flow is given in Figure 1. We developed a bioimpedance acquisition system and performed a pilot study including ten healthy subjects. While simulating a short load we recorded both the impedance at the forearm and a pneumotachometer (PNT) reference. Using PPG fiducial points, we extracted seven time-domain features from the impedance signal. Employing four different regression models, we estimated the respiratory flow \hat{Q} as well as the respiratory rate (RR) from an optimal subset of the features. We implemented a model and feature selection framework to find optimal feature sets and model orders. The RR estimation was performed using the maximum of the DFT in the range of 6 to 36 breaths per minutes (bpm) in 20 s frames with 50 % overlap from the fitted signals.

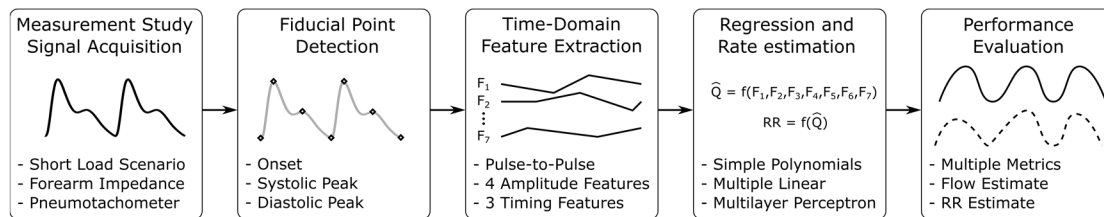


Figure 1. Methodological overview of the signal flow in the presented work.

2.2 Acquisition System

We developed a versatile bioimpedance measurement system based on our robust wireless body sensor network (rBSN) (Pflugradt, Mann, Tigges, Görnig, & Orglmeister, 2016). We employed an AD5933 impedance converter system which we extended by a bridged Howland current source output and an instrumentation amplifier input with 0.69 Hz error integrator feedback. We were thus able to realize tetrapolar current injection measurement schemes of frequencies between 1 kHz and 100 kHz with peak currents of 1 μ A to 1 mA. The complex impedance measurement is carried out at 500 samples/s in both amplitude and phase. To provide a respiratory reference, we included a pneumotachometer (PNT) system into our measurement setup. The respiratory flow was acquired highly synchronous to the impedance measurements at 500 samples/s. The power drawn by the full system remains below 100 mW in all conditions at a system voltage of 3.3 V.

2.3 Pilot Study Design and Signal Pre-Processing

We conducted a measurement study including ten healthy subjects (4 female) aged 26.5 ± 3.3 years. We simulated a short load scenario in a 12 minutes long course including a four minutes long rest, a one minute long light load and a seven minutes recovery period. The load period was implemented using a bicycle ergometer with a loading of 25 W. To acquire the IPG in a tetrapolar measurement scheme we attached four disposable, self-adhesive Ag/AgCl electrodes to the forearm as shown in Figure 2. The two inner measurement electrodes were spaced 10 cm apart center-to-center. The impedance measurements were carried out at a frequency of 100 kHz with 900 μ A peak current.

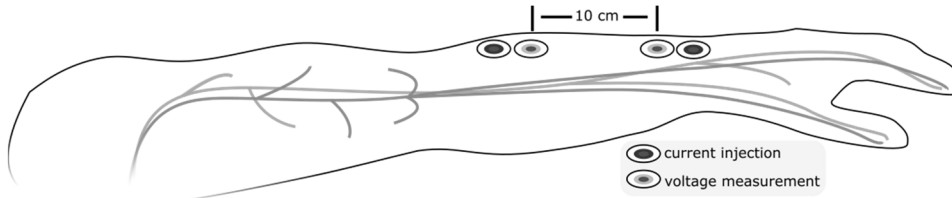


Figure 2. The position of the current injection and voltage measurement electrodes on the forearm.

The recorded IPG signals were low-pass filtered with a cut-off frequency of 35 Hz. We removed baseline wandering by subtracting a 7500 point gliding mean filtered (GMF) version of the original signal which corresponds to a 0.03 Hz high-pass filter. Finally, the resulting signal was smoothed using a 350 point GMF resulting in an approximate low-pass cutoff frequency of 0.63 Hz. The reference PNT signal was handled in the same manner. Using pattern matching techniques (Orphanidou, et al., 2015), we automatically assessed the quality of the signal and rejected ill-conditioned sections.

2.4 Vascular Impedance Plethysmographic Signals and Features

The vascular IPG is an impedance-based method of acquiring plethysmographic information from the vessels of the peripherals. The acquired waveforms are similar in both shape and interpretability to the widely known PPG waveforms. Therefore, the IPG signal analysis can be performed using well established fiducial points and features from the PPG signal analysis. We used the fiducial points pulse onset, systolic peak and diastolic peak as visualized in Figure 3 (a) for the feature calculation. The pulse onset was derived using the widely used open-source algorithm for arterial blood pressure signals proposed by Zong et al. (Zong, Heldt, Moody, & Mark, 2003). The systolic peak was then defined as the maximum value between two consecutive pulse onsets. The diastolic peak is derived using the minimum of the second derivative of the pulse signal section between the systolic peak and the next pulse onset (Millasseau, Kelly, Ritter, & Chowienczyk, 2002).

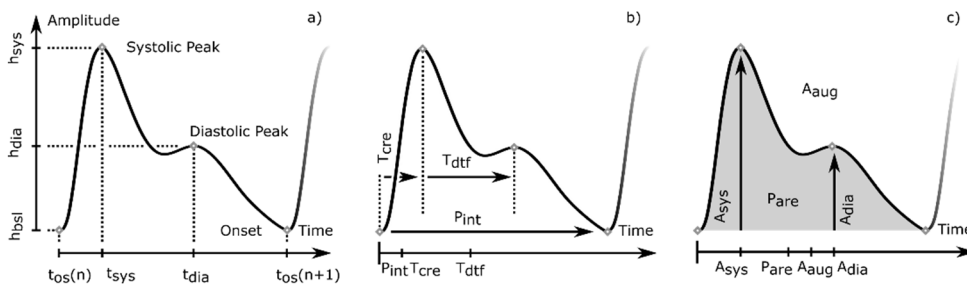


Figure 3. a) Fiducial points of peripheral plethysmography signals. b) Timing features. c) Amplitude features.

Based on the three fiducial points we calculated seven time-domain features which can be categorized into amplitude and timing features (Elgendi, 2012). The decision to stay in the time domain was motivated by the wearable use case and allows us to calculate, fuse and evaluate the feature vectors in low-power embedded environments without excessive computational burden. The features and their positions within the pulse curve are visualized in Figure 3 (b, c) and their calculation based on the fiducial points is given in Table 1. Please note that the position of the features in the pulse is also calculated individually for every feature. Thus the temporal resolution of the resulting estimation is potentially increased when multiple features are combined.

Table 1. Time domain features of the plethysmography signal employed for estimating respiratory flow and rate.

Feature Nr.	Names	Symbol	Calculation	Time in pulse n
1	Systolic Amplitude	A_{sys}	$h_{sys}(n) - h_{bsl}(n)$	$t_{os}(n) + t_{sys}(n)$
2	Diastolic Amplitude	A_{dia}	$h_{dia}(n) - h_{bsl}(n)$	$t_{os}(n) + t_{dia}(n)$
3	Augmentation Index	A_{aug}	$\frac{h_{dia}(n)}{h_{sys}(n)}$	$t_{os}(n) + \frac{t_{dia}(n) - t_{sys}(n)}{2}$
4	Pulse Area	P_{are}	$\int (Pulse - h_{bsl}(n)) dt$	$t_{os}(n) + \frac{t_{os}(n+1) - t_{os}(n)}{2}$
5	Pulse Interval	P_{int}	$t_{os}(n+1) - t_{os}(n)$	$t_{os}(n)$
6	Crest Time	T_{cre}	$t_{sys}(n) - t_{os}(n)$	$t_{os}(n) + \frac{t_{sys}(n) - t_{os}(n)}{2}$
7	Delta-T Feature	T_{dtf}	$t_{dia}(n) - t_{sys}(n)$	$t_{os}(n) + \frac{t_{dia}(n) - t_{sys}(n)}{2}$

where

- h_{sys} = amplitude of the systolic peak
- h_{bsl} = amplitude of the baseline
- h_{dia} = amplitude of the diastolic peak
- t_{os} = position of the onset in the pulse
- t_{sys} = position of the systolic peak in the pulse
- t_{dia} = position of the diastolic peak in the pulse.

To estimate the respiratory signal from the features presented in Table 1, we first up-sampled the feature vectors to the system sample frequency of 500 Hz by simple linear interpolation. Since the presented features vary with the lung volume and our used PNT reference is a respiratory flow Q , we first differentiated the feature vectors to receive flow dependent feature vectors. The differentiated feature signals were filtered using the same parameters as discussed in the signal preprocessing step, resulting in $n = 7$ raw feature vectors F_n^r . Finally, the feature vectors were individually normalized using the z-score as given in Equation 1, resulting in $n = 7$ normalized, flow dependent feature vectors F_n . In theory, there are 127 possible feature vector sets with $n = 7$ available features. Each normalized feature set is defined as a feature set matrix F_{set} as given in Equation 2, for instance, the matrix $F_{1,3,7} = [F_1, F_3, F_7]$ containing the individually normalized, differentiated and filtered vectors of the features 1, 3 and 7:

$$F_n = \frac{F_n^r - \overline{F_n^r}}{\text{Var}(F_n^r)}, \forall n \in [1, 7], \quad (1)$$

and

$$F_{set} \subseteq \{F_1, F_2, F_3, F_4, F_5, F_6, F_7\}, \quad (2)$$

where

- F_n = normalized filtered differentiated feature vector n ,
- F_n^r = filtered differentiated feature vector n ,
- F_{set} = feature set matrix containing the z-score normalized feature vectors for the current set.

2.5 Regression Models

After extracting the feature vectors from the IPG signal using the discussed fiducial points, we derived regression functions between the features and the respiratory flow employing four different models: simple polynomial regression, multiple linear regression using polynomial models and multilayer perceptrons (MLP) with two and three hidden layers. Figure 5 exemplary shows the IPG waveform with fiducial points (a), the normalized feature vectors (b-d) as well as the estimated and reference flow signals (e). In the following, the different models are described in more detail.

Simple Polynomial Regression with Averaged Feature Vectors

In the case of the simple polynomial fit we first calculated \bar{F}_{set} as the one-dimensional average of the z-score normalized feature vectors contained in a feature subset *set* as given in Equation 3. Please note that the averaging of the normalized feature vectors is performed over the vectors defined in the subset *set* and not along the time domain, thus implementing a low-complexity, linear time-domain feature fusion step which can be easily transferred to any embedded system with limited computational resources. The resulting fused feature vector \bar{F}_{set} is then fitted to the reference flow Q using polynomial models as given in Equation 4 to retrieve an estimated respiratory flow \hat{Q} . We analyzed polynomial regression models up to the order of $M=20$.

$$\bar{F}_{set} = \frac{1}{nSet} \sum_{j \in set} F_j, set \subseteq \{1, 2, \dots, 7\}, \quad (3)$$

and

$$\hat{Q} = \sum_{i=0}^M a_i \bar{F}_{set}^i, \quad (4)$$

where

- \bar{F}_{set} = one-dimensional average of the z-score normalized feature vector set,
- F_j = normalized feature vector j,
- set* = a subset of feature numbers from the full set of normalized feature vectors,
- nSet* = number of features vectors selected by *set*,
- \hat{Q} = estimated flow signal,
- a_i = parameters of the polynomial,
- M = order of the polynomial.

Multiple Linear Regression using Polynomial Models

By employing multiple linear regression, we fused the features and performed the regression in a single step. We used polynomial model functions within the linear regression up to the order of $M=20$ in the form given in Equation 5. The used model did not contain cross terms between features:

$$\hat{Q} = a_0 + \sum_{i=1}^M \sum_{j \in set} a_{ij} F_j^i, set \subseteq \{1, 2, \dots, 7\}, \quad (5)$$

where

- \hat{Q} = estimated flow signal,
- a_0 = constant parameter of the model,
- M = order of the polynomials,
- set* = a subset of feature numbers from the full set of normalized feature vectors,
- a_{ij} = parameter for the i^{th} power of the j^{th} feature vector,
- F_j^i = normalized feature vector j to the power of i.

An example polynomial is given in Equation 6 for the feature subset $set = \{1, 3, 7\}$ and the polynomial order $M = 2$, thus using three features with second order polynomials in the multiple linear regression. Please note the absence of cross terms:

$$\hat{Q} = a_0 + a_{11}F_1 + a_{21}F_1^2 + a_{13}F_3 + a_{23}F_3^2 + a_{17}F_7 + a_{27}F_7^2, \quad (6)$$

where

the nomenclature follows that of Equation 5.

Multilayer Perceptron Regression

We evaluated the regression performance of feed-forward multi-layer perceptrons (MLP) as given in Figure 4. We used the MLP to fuse the available feature vectors and perform the regression in a single step. We evaluated the MLPs with two and three hidden layers with up to 20 neurons per layer. All hidden layer neurons use sigmoid activation functions.

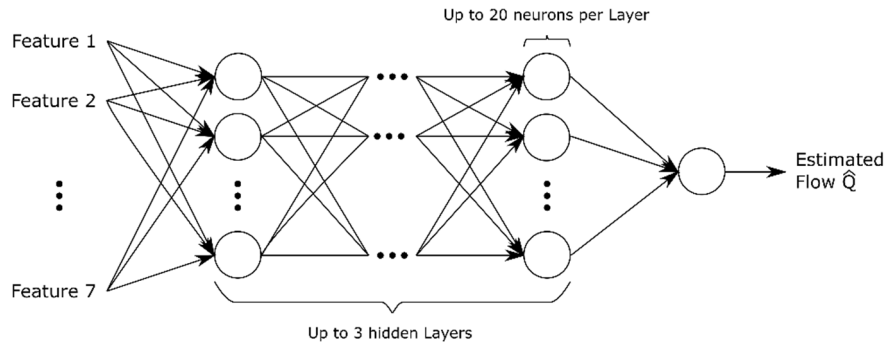


Figure 4. Structure of the multilayer perceptron. We used up to three hidden layers and up to 20 neurons per layer. The number of inputs depends on the feature selection.

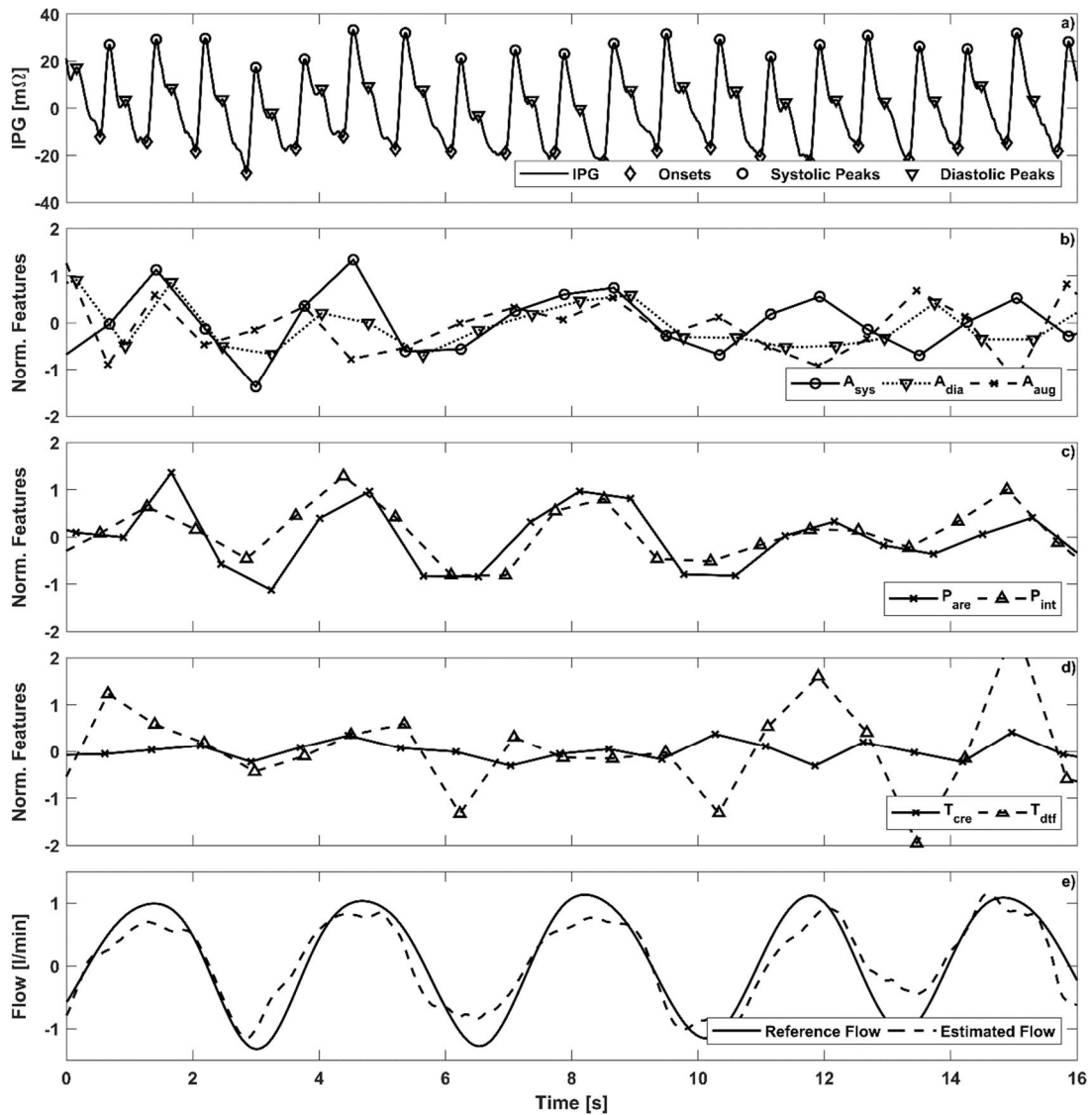


Figure 5. Example signals. a) IPG and fiducial points. b-d) Linearly interpolated, normalized feature vectors. The markers indicate the positions of the respective features in the pulse. e) Reference and estimated flow.

2.6 Performance Metrics

We assessed the performance of the resulting fit between the surrogate flow \hat{Q} and the reference flow Q using five metrics and their standard deviations. First, the linear correlation between the flow surrogate and reference is calculated using the Pearson's linear correlation coefficient r as given in Equation 7. The systematic error or bias is evaluated using the mean error (ME) given in Equation 8. In addition, we calculated the mean absolute error (MAE) given in Equation 9, and the relative metric normalized root mean squared error ($NRMSE$) in percent as given in Equation 10.

For the feature selection process, the mean squared error (MSE) as given in Equation 11 was employed. To compare the different regression models, we utilized the Bayesian information criterion (BIC) (Schwarz, 1978) as given in Equation 12. We have chosen the BIC over the Akaike Information Criterion (AIC) (Akaike, 1998), as given in Equation 13, due to its reduced tendency to select a large model in the event of a large number of observations N . Both quantities are based on the sum of squared errors (SSE) given in Equation 14:

$$r = \frac{\sum_{i=1}^N (\hat{Q}(i) - \bar{\hat{Q}})(Q(i) - \bar{Q})}{\sqrt{\sum_{i=1}^N (\hat{Q}(i) - \bar{\hat{Q}})^2} \sqrt{\sum_{i=1}^N (Q(i) - \bar{Q})^2}} \quad (7)$$

$$ME = \frac{\sum_{i=1}^N \hat{Q}(i) - Q(i)}{N}, \quad (8)$$

$$MAE = \frac{\sum_{i=1}^N |\hat{Q}(i) - Q(i)|}{N}, \quad (9)$$

$$NRMSE = \frac{\sqrt{\frac{\sum_{i=1}^N [\hat{Q}(i) - Q(i)]^2}{N}}}{\frac{\sum_{i=1}^N |Q(i)|}{N}} * 100, \quad (10)$$

$$MSE = \frac{\sum_{i=1}^N (\hat{Q}(i) - Q(i))^2}{N}, \quad (11)$$

$$BIC = N \ln\left(\frac{SSE}{N}\right) + \ln(N) K, \quad (12)$$

$$AIC = N \ln\left(\frac{SSE}{N}\right) + 2K, \quad (13)$$

$$SSE = \sum_{i=1}^N (\hat{Q}(i) - Q(i))^2, \quad (14)$$

where

- r = Pearson's linear correlation coefficient,
- \hat{Q} = estimated flow signal [l/min],
- Q = reference flow signal [l/min],
- ME = mean error (bias) [l/min],
- MAE = mean absolute error [l/min],
- $NRMSE$ = normalized root mean squared error [%],
- BIC = Bayes information criterion,
- N = number of observations,
- SSE = sum of squared errors [l²/min²],
- K = order of the model + 1,
- BIC = Bayesian information criterion,
- AIC = Akaike information criterion.

2.7 Model and Feature Selection Framework

The regression model and feature selection were implemented using a nested cross-validation framework as shown in Figure 6. To parametrize the data division and the number of validation rounds individually and potentially reduce the computational burden, Monte Carlo cross-validation (MCCV), also known as repeated random sub-sampling validation (Picard & Cook, 1984) has been chosen over k -fold cross-validation.

The outer MCCV divides the dataset into training and test samples with a ratio of 90:10. For all d outer MCCV validation rounds, the k regression models are passed with increasing model order to the underlying forward feature wrapper with the m features given in Table 1. The inner MCCV divides the training data of the outer MCCV again into a 90:10 subset. For each of the p inner validation rounds, the current regression model is trained using the current feature set of the forward feature wrapper.

The resulting p trained regression models are evaluated inside the inner MCCV and the performance values, in the presented architecture the MSE, are averaged. If a newly added feature to the feature set does not increase the performance, the forward feature wrapper passes the last feature set as best performing combination for the current regression model. Likewise, if a model-feature combination does not decrease the BIC, the previous model-feature combination is returned as an optimum. Finally, the d optimal model-feature combinations are evaluated using the outer MCCV test data, resulting in d cross-validated performance measures which were averaged. In addition, the distribution of the selected features was evaluated.

We performed the model and feature selection in four distinct categories: simple polynomial models, multiple linear regression using polynomial models, MLPs with two hidden layers and MLPs with three hidden layers. For each of the four model categories, the described framework was used to find the optimal model order concerning the BIC and the accompanying feature set. For the framework parameters, we chose $d = 12$ and $p = 2$. The parameter m was 7 due to the seven used features.

3. Results

3.1 Model and Feature Selection

We first analyzed the optimal model order for each of the four models individually. As shown in Figure 7, the optimal order of the simple polynomial regression model with averaged features was found to be 9. Please note that the polynomial regression models of order 1 and 2 were excluded from the graph due to their BIC of an order of magnitude above all shown regression models. The multiple linear regression using polynomial models had an optimal polynomial order of 10. The BIC difference to the optimal simple polynomial regression was $11 * 10^3$. For the MLP with two hidden layers the optimal neurons per hidden layer were 7 which sums up to a total of 14 neurons. The BIC difference to the optimal multiple linear regression model was $7.1 * 10^3$. Evaluating the MLP models with three hidden layers, an optimum was found using 12 neurons per layer giving a total of 36 neurons. The BIC difference to the optimal MLP model with two hidden layers was $4.4 * 10^3$. Thus when compared against each other, the MLP regression model with three hidden layers and 12 neurons per layer are found to be optimal. The MLP with two hidden layers outperformed the multiple regression model at the same number of parameters. The standard deviations of the BIC were small in all cases.

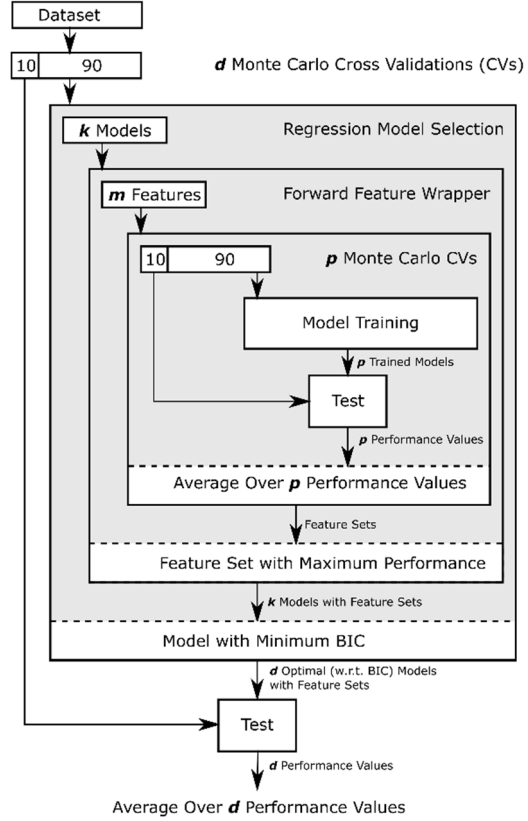


Figure 6. Model and feature selection framework using nested Monte Carlo cross-validation and a forward feature wrapper.

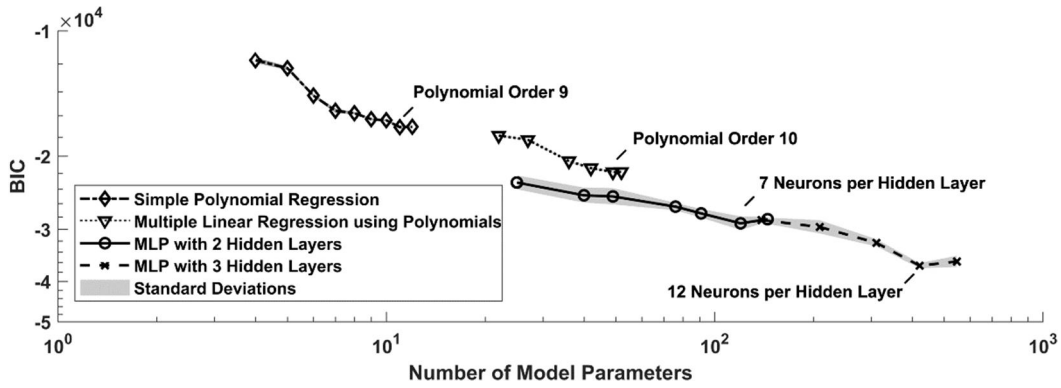


Figure 7. BIC for analyzed regression models. The found optimum in model size concerning the BIC is given per model type. An optimum across all four model classes is found using MLPs with three hidden layers.

For the simple polynomial regression models with averaged feature vectors, the forward feature wrapper consistently returned the single feature P_{int} , the pulse interval, over all other combinations. No other feature combination was returned in any order of the polynomial except for order 1 and 2. In these low order models, the framework returned the combination P_{int} , T_{dtf} , A_{sys} .

In Table 2 the feature selection results for the MLP and multiple linear regression models are summarized. The feature P_{int} was selected in the first place every time, followed by the T_{dtf} feature which was selected second 97,6 % of the time. The A_{aug} feature was selected third 63,4 % of the time. The features P_{are} and A_{dia} were not selected in 4,9 % and 22,0 % of the cases respectively. The framework returned at least five features every time and six features 97,6 % of the time. In 75,6 % of the cases, all features have been selected.

Table 2. Selection of features for every position in the feature sequence returned by the forward wrapper in percent. The proportion of a position being used is given in the last column. The last row shows the percentage of the individual features not being selected in any position.

Feature Position	P_{int} [%]	T_{dtf} [%]	A_{aug} [%]	A_{sys} [%]	T_{cre} [%]	P_{are} [%]	A_{dia} [%]	Position Used [%]
1 st	100,0	0,0	0,0	0,0	0,0	0,0	0,0	100,0
2 nd	0,0	97,6	2,4	0,0	0,0	0,0	0,0	100,0
3 rd	0,0	0,0	63,4	9,8	14,6	4,9	7,3	100,0
4 th	0,0	0,0	24,4	31,7	2,4	41,5	0,0	100,0
5 th	0,0	2,4	4,9	7,3	65,9	17,1	2,4	100,0
6 th	0,0	0,0	4,9	36,6	12,2	24,4	19,5	97,6
7 th	0,0	0,0	0,0	14,6	4,9	7,3	48,8	75,6
Not Selected	0,0	0,0	0,0	0,0	0,0	4,9	22,0	

3.2 Respiratory Flow Estimation

The estimation performances using the optimal feature set for the respective models are given in Table 3. Please note that for the simple polynomial regression model, the optimal feature set selected was the single feature P_{int} . We additionally analyzed possible performance increases using the three other models in conjunction with the single feature P_{int} but found no significant improvements. Using the higher order models with their respective optimal feature sets however increased the flow estimation performance significantly as shown in Table 3. By employing the MLP regression model with three hidden layers, a relative error of 59 % and a linear correlation of $0,85 \pm 0,005$ was achieved.

Table 3. Performance of the respiratory flow estimation for simple polynomial models, multiple linear regression using polynomial models and MLP regression models using the respective optimal feature sets.

Regression Model	ME [l/min]	MAE [l/min]	MSE [l ² /min ²]	NRMSE [%]	r
Simple Polynomial Regression	-0,005±0,005	0,617±0,002	0,592±0,004	87,7±0,3	0,640±0,003
Multiple Linear Regression	0,002±0,004	0,545±0,003	0,483±0,004	79,3±0,4	0,720±0,004
MLP with 2 Hidden Layers	-0,003±0,002	0,381±0,005	0,252±0,005	71,6±0,6	0,779±0,005
MLP with 3 Hidden Layers	-0,002±0,000	0,317±0,004	0,177±0,006	59,4±1,00	0,851±0,005

3.3 Respiratory Rate Estimation

Using each of the four regression model classes, we estimated the respiratory rate. In Figure 8 an exemplary Bland-Altman plot is shown for an MLP regression model with three hidden layers and 12 neurons each. All seven features have been used in the regression model. The relative error was 1.6 %. The plot shows a next to zero mean and a slight proportional bias. The standard deviation of the error is shown to be 0.2 bpm, and the correlation is 0.998. No dependent error deviation was found over the range of 5 to 25 bpm.

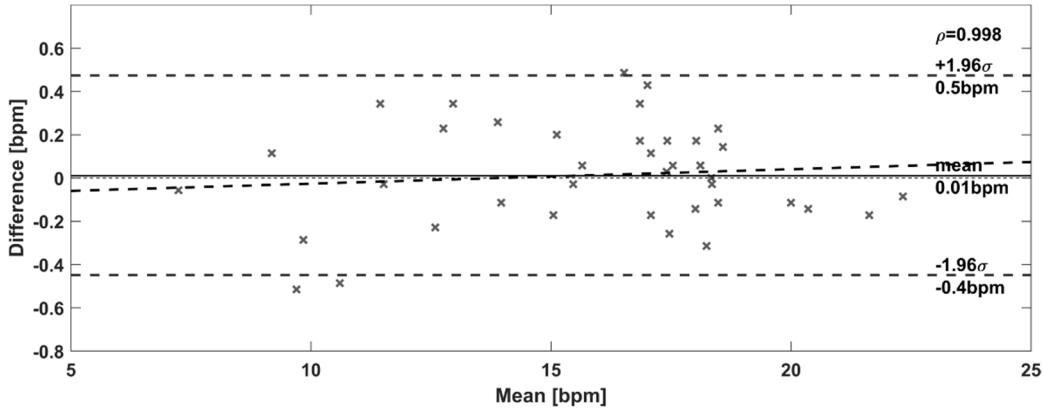


Figure 8. Exemplary Bland-Altman plot of the respiratory rate estimation using an MLP with three hidden layers.

The performance of the respiratory rate estimation using the optimal feature sets for the respective models is given in Table 4. Please note that for the simple polynomial regression model, the optimal feature set selected was the single feature P_{int} . In this case, the relative error was about 14 % with a ME of -0.44 bpm and a MAE of 0,745 bpm. Using the MLP model with three hidden layers, we were able to significantly increase the performance to a ME of -0.01 bpm, a MAE of 0.2 ± 0.2 bpm and a relative error of 1.5 %.

Table 4. Performance of the respiratory rate estimation using the estimated flow signals from polynomial and MLP regression.

Regression Model	ME [bpm]	MAE [bpm]	NRMSE [%]
Simple Polynomial Regression	-0,440±2,187	0,745±2,101	13,9±0,0
Multiple Linear Regression	0,017±0,056	0,334±0,061	3,5±1,6
MLP with 2 Hidden Layers	0,024±0,406	0,282±0,290	2,4±0,1
MLP with 3 Hidden Layers	-0,012±0,025	0,164±0,182	1,5±0,1

4. Discussion and Limitations

4.1 Model and Feature Selection

The model selection showed a trend towards higher order nonlinear models. While first and second order polynomials performed an order of magnitude worse than other models we found an acceptable simple polynomial optimum at the order 9. In the case of multiple linear regression using polynomial models an optimal order of 10 was found. The higher order MLP models did perform significantly better. However, their complexity is between one and two orders of magnitude larger than those of the polynomial approaches. The optimal model concerning the BIC of all four model categories was an MLP with three hidden layers and 12 neurons in each layer, which had about 400 parameters. In the author's opinion, it remains debatable if such a high model order is justified for the presented problem.

In the feature selection step, the selected features for the lower order simple polynomial models have been the combination of P_{int} , T_{dtf} and A_{sys} . This is consistent with our previous work on respiratory rate estimation from vascular impedance plethysmography (Klum, Osterland, Pielmus, Tigges, & Orglmeister, 2018). However, for higher simple polynomial model orders the only selected feature was P_{int} . It was expected that this feature would be amongst the best performing due to its close relation to the heart rate and thus the respiratory sinus arrhythmia. The fact, however, that higher polynomial models tended to discard the other features leads to the assumption that a simple linear combination of the normalized feature vectors is not the optimal way to fuse the features prior to the polynomial regression. Employing multiple linear regression using polynomial models we extended the simple polynomial regression approach. We found significant improvements in performance and model selection results similar to the MLP case.

In both the multiple linear regression and MLP regression approaches the feature selection was largely homogeneous amongst the models. The feature P_{int} was returned first in all cases. The T_{dtf} feature, the time between systolic and diastolic peak, was returned in almost all cases as the second feature. We hypothesize this to be a result of the respiratory influence on the vasoconstriction and thus pulse wave velocity, which in turn modulates the distance between systolic and diastolic peak. The A_{aug} feature, representing the quotient of a diastolic and systolic peak, is consistently selected the third feature 63,4 % of the time. Again, a relation between respiration and vasoconstriction could be a possible explanation. Being not selected 22 % of the time, the A_{dia} feature which represents the amplitude of the diastolic peak was the least optimal. The feature selection step tended towards selecting most if not all of the features in the multiple linear and MLP regression model cases. We propose this to be a result of the different features being located at different positions within the pulse, thus increasing the temporal resolution of the estimate with an increasing number of features.

4.2 Respiratory Flow and Rate Estimation

Using simple polynomial models with the single feature P_{int} we were able to estimate the respiratory flow with a relative error of down to 87,8 %. Using the multiple linear regression or MLP regression models did not increase the performance in the single feature case in any configuration. In contrast, when using the respective optimal feature sets, we were able to decrease the relative error to 59 % for MLPs with three hidden layers. The results indicate that a nonlinear fusion of multiple features can significantly increase the regression performance. Nonlinear regression of single features is less than optimal.

Using the estimated flow signals we were able to obtain RR estimation errors of down to 14 % for the simple polynomial case with the single feature P_{int} . Using MLP models with the optimal feature sets, we were able to reduce the error to 1.5 % with a close to zero bias. Thus, fusing additional features in a nonlinear way lead to a significant increase in performance both in flow and RR estimation, which we explain both by the increase in temporal resolution of the resulting signal and additional information content as theorized in the cases of the features T_{dtf} and A_{aug} .

4.3 Limitations

The most important limitation of the presented work is the data basis. We used a bicycle ergometer to simulate a typical short load scenario. Even though we were able to evoke natural and physiological variations of breathing rate and depth over a wide range, the movement artifacts imposed by the physical activity degraded the signals. In addition, it cannot be excluded that the changing activity over the course of the pilot study had an impact on the extracted features.

The feature and model selection framework is limited in the sense that both the selected regression models and feature combinations can represent local minima. This is a result of the strict implementation that the first minimum is used as the optimum in both cases.

5. Summary and Conclusion

Our aim was to estimate the respiratory flow and rate from impedance plethysmography signals acquired at the forearm. Using seven time-domain features, we compared simple polynomial regression, multiple linear regression using polynomial models and multilayer perceptrons (MLP) with two and three layers for the estimation of the respiratory signal. We developed a model and feature selection framework to assess the optimal model order concerning the Bayesian Information Criterion and the optimal feature set using a forward wrapper approach. Overall, a three-layered MLP with twelve neurons per layer performed best. The pulse interval was the optimal feature, followed by the delta-t feature and the augmentation index. The framework tended to select at least five of the seven presented features. The diastolic amplitude was selected least common. Using MLPs, the respiratory flow estimation error was 59 % with a relative error in the respiratory rate estimation of 1.5 %.

We conclude that respiratory rate estimation is possible to a high degree of accuracy using impedance plethysmographic signals obtained from the forearm. Estimating the respiratory flow using only time domain features from the impedance plethysmography requires high order nonlinear models and a nonlinear feature fusion step. The shown accuracies would allow apnea detection but need additional optimization for more advanced tasks.

Abbreviations

AIC	Akaike Information Criterion
BIC	Bayes Information Criterion
bpm	Breaths Per Minute
DFT	Digital Fourier Transform
ECG	Electrocardiogram
GMF	Gliding Mean Filter
IPG	Impedanceplethysmogram
MCCV	Monte Carlo Cross Validation
MAE	Mean Absolute Error
ME	Mean Error
MLP	Multilayer Perceptron
MSE	Mean Squared Error
NRMSE	Normalized Root Mean Squared Error
PNT	Pneumotachometer
PPG	Photoplethysmogram
RR	Respiratory Rate
IP	Impedance Pneumography
IPG	Impedanceplethysmogram

Bibliography

- Akaike, H. (1998). Information theory and an extension of the maximum likelihood principle. In *Selected papers of hirotugu akaike* (pp. 199-213). Springer.
- Anderson, F. A. (1984). Impedance plethysmography in the diagnosis of arterial and venous disease. *Annals of biomedical engineering*, *12*, 79-102.
- Broens, S. J., He, X., Evley, R., Olofsen, E., Niesters, M., Mahajan, R. P., . . . Velzen, M. (2017). Frequent respiratory events in postoperative patients aged 60 years and above. *Therapeutics and clinical risk management*, *13*, 1091.
- Brown, B. H., Pryce, W. I., Baumber, D., & Clarke, R. G. (1975). Impedance plethysmography: can it measure changes in limb blood flow. *Medical and biological engineering*, *13*, 674-682.
- Cardinale, M., & Varley, M. C. (2017). Wearable training-monitoring technology: Applications, challenges, and opportunities. *International journal of sports physiology and performance*, *12*, S2--55.
- Charlton, P. H., Bonnici, T., Tarassenko, L., Clifton, D. A., Beale, R., & Watkinson, P. J. (2016). An assessment of algorithms to estimate respiratory rate from the electrocardiogram and photoplethysmogram. *Physiological measurement*, *37*, 610.
- Cho, M.-C., Kim, J.-Y., & Cho, S. (2009). A bio-impedance measurement system for portable monitoring of heart rate and pulse wave velocity using small body area. *Circuits and Systems, 2009. ISCAS 2009. IEEE International Symposium on*, (pp. 3106-3109).
- Cornet, V. P., & Holden, R. J. (2018). Systematic review of smartphone-based passive sensing for health and wellbeing. *Journal of biomedical informatics*, *77*, 120-132.

- Elgendi, M. (2012). On the analysis of fingertip photoplethysmogram signals. *Current cardiology reviews*, 8, 14-25.
- Hertleer, C., Odhiambo, S., & Van Langenhove, L. (2013). Protective clothing for firefighters and rescue workers. In *Smart textiles for protection* (pp. 338-363). Elsevier.
- Huynh, T., Jafari, R., & Chung, W.-Y. (2018). An Accurate Bioimpedance Measurement System for Blood Pressure Monitoring. *Sensors*, 18, 2095.
- Jaffrin, M. Y., & Vanhoutte, C. (1979). Quantitative interpretation of arterial impedance plethysmographic signals. *Medical and Biological Engineering and Computing*, 17, 2-10.
- Jivet, I. (2014). Wrist pulse monitoring by electrical impedance using a 3D model of the arm. *Electronics and Telecommunications (ISETC), 2014 11th International Symposium on*, (pp. 1-4).
- Klum, M., Minn, T., Tigges, T., Pielmus, A.-G., & Orglmeister, R. (2016). Minimally spaced electrode positions for multi-functional chest sensors: ECG and respiratory signal estimation. *Current Directions in Biomedical Engineering*, 2, 695-699.
- Klum, M., Osterland, D., Pielmus, A.-G., Tigges, T., & Orglmeister, R. (2018). Peripheral Vascular Impedance Plethysmography for Respiratory Rate Estimation using Beat-to-Beat Features. *International Journal of Bioelectromagnetism*, 20, 43-46.
- Klum, M., Schenck, T., Pielmus, A., Tigges, T., & Orglmeister, R. (2018). Short Distance Impedance Pneumography. *Current Directions in Biomedical Engineering*, 4, 109-113.
- Marks, L. A. (1987). Digital enhancement of the peripheral admittance plethysmogram. *IEEE transactions on biomedical engineering*, 192-198.
- Millasseau, S. C., Kelly, R. P., Ritter, J. M., & Chowienczyk, P. J. (2002). Determination of age-related increases in large artery stiffness by digital pulse contour analysis. *Clinical science*, 103, 371-377.
- Nyboer, J., Kreider, M. M., & Hannapel, L. (1950). Electrical impedance plethysmography: A physical and physiologic approach to peripheral vascular study. *Circulation*, 2, 811-821.
- Orphanidou, C., Bonnici, T., Charlton, P., Clifton, D., Vallance, D., & Tarassenko, L. (2015). Signal-quality indices for the electrocardiogram and photoplethysmogram: Derivation and applications to wireless monitoring. *IEEE journal of biomedical and health informatics*, 19, 832-838.
- Pflugradt, M., Mann, S., Tigges, T., Görnig, M., & Orglmeister, R. (2016). Multi-modal signal acquisition using a synchronized wireless body sensor network in geriatric patients. *Biomedical Engineering/Biomedizinische Technik*, 61, 57-68.
- Picard, R. R., & Cook, R. D. (1984). Cross-validation of regression models. *Journal of the American Statistical Association*, 79, 575-583.
- Ramasamy, M., Oh, S., Harbaugh, R., & Varadan, V. K. (2013). Real time monitoring of driver drowsiness and alertness by textile based nanosensors and wireless communication platform. *Forum for Electromagnetic Research Methods and Application Technologies (FERMAT) 2013*.
- Rose, D. K., Cohen, M. M., Wigglesworth, D. F., & DeBoer, D. P. (1994). Critical respiratory events in the postanesthesia care unit. Patient, surgical, and anesthetic factors. *Anesthesiology*, 81, 410-418.
- Schneider, J., Schroth, M., Holzhey, M., Blöcher, T., & Stork, W. (2017). An approach to improve impedance plethysmography on the wrist by using adaptive feedback control. *Sensors Applications Symposium (SAS), 2017 IEEE*, (pp. 1-6).
- Schneider, J., Schroth, M., Ottenbacher, J., & Stork, W. (2018). A novel wearable sensor device for continuous monitoring of cardiac activity during sleep. *Sensors Applications Symposium (SAS), 2018 IEEE*, (pp. 1-6).
- Schwan, H. P. (1955). Electrical properties of body tissues and impedance plethysmography. *IRE Transactions on Medical Electronics*, 32-46.
- Schwarz, G. (1978). Estimating the dimension of a model. *The annals of statistics*, 6, 461-464.
- Sun, Z., Sessler, D. I., Dalton, J. E., Devereaux, P. J., Shahinyan, A., Naylor, A. J., . . . others. (2015). Postoperative hypoxemia is common and persistent: a prospective blinded observational study. *Anesthesia and analgesia*, 121, 709.
- Tal, A., Shinar, Z., Shaki, D., Codish, S., & Goldbart, A. (2017). Validation of contact-free sleep monitoring device with comparison to polysomnography. *Journal of Clinical Sleep Medicine*, 13, 517-522.
- Varaki, E. S., Gargiulo, G. D., Penkala, S., & Breen, P. P. (2018). Peripheral vascular disease assessment in the lower limb: A review of current and emerging non-invasive diagnostic methods. *Biomedical engineering online*, 17, 61.

- Zeng, W., Shu, L., Li, Q., Chen, S., Wang, F., & Tao, X.-M. (2014). Fiber-based wearable electronics: a review of materials, fabrication, devices, and applications. *Advanced Materials*, 26, 5310-5336.
- Zong, W., Heldt, T., Moody, G. B., & Mark, R. G. (2003). An open-source algorithm to detect onset of arterial blood pressure pulses. *Computers in Cardiology*, 2003, (pp. 259-262).